PCCP

Accepted Manuscript

ROYAL SOCIETY OF CHEMISTRY

www.rsc.org/pccp

Direct Dynamic Nuclear Polarization Targeting Catalytically Active ^{27}Al Sites

Alicia Lund,[a] Ming-Feng Hsieh,[b] Ting-Ann Siaw,[a] Song-I Han [a,b]

[a] Department of Chemistry and Biochemistry University of California Santa Barbara, Santa Barbara, CA 93106-9510
[b] Department of Chemical Engineering University of California Santa Barbara, Santa Barbara, CA 93106-5080

Abstract

Here we present a systematic study of direct ^{27}Al Dynamic Nuclear Polarization (DNP) as induced using three different mono-radical probes with side groups of varying charge states. By employing 4-amino TEMPO that adsorbs to negatively charged surface sites of Al-SBA-15, we achieve a ^{27}Al signal enhancement factor of ~13 compared to a signal enhancement factor of ~3-4 from mono-radicals that do not adsorb as strongly to the surfaces of Al-SBA-15, here 4-carboxy and 4-hydroxy TEMPO. By performing Electron Spin Echo Envelope Modulation (ESEEM) experiments and continuous wave (cw) Electron Paramagnetic Resonance (EPR) lineshape analysis with the various nitroxide probes imbibed in Al-SBA-15, we find that direct ^{27}Al DNP enhancements achieved with different spin probes can be attributed to proximity and local concentration of the spin probes to the aluminum on the surface of the mesoporous alumina-silica.

Introduction

Mesoporous alumina-silica materials have great industrial potential to facilitate acid catalyzed reactions such as dehydration–condensation, alkylation, and isomerization processes.[1–3] These mesostructured materials have attracted interest due to their high surface area and large pore sizes (10-100 nm) to host polymers and other bulky reactants.[4,5] Solid-state NMR (ssNMR) spectroscopy in combination with magic angle spinning (MAS) is already an important tool for elucidating the atomic-level structure of heterogeneous porous material, including alumina-silicas such as Al-SBA-15.[6,7] However, the inherently low signal sensitivity of NMR makes it exceptionally difficult to selectively examine surface species, especially the catalytically active aluminum centers that are even more dilute than the surface matrix species. This is all complicated by the spectral broadening of the aluminum spins that arise from the quadrupolar interaction, S=5/2 for ^{27}Al, that can reduce the NMR signal of surface aluminum species

to an undetectable limit.[8] Griffin and co-workers' development of dynamic nuclear polarization (DNP) at high magnetic fields, under MAS and liquid nitrogen temperatures achieved up to two orders of magnitude of signal enhancement, i.e. shortening the acquisition time of ssNMR spectra by up to four orders of magnitude.[9] This method of enhancing NMR signal has been shown to be one of the most effective NMR methods for obtaining surface enhanced NMR spectra.[10]

Recently, DNP methods have been applied in order to obtain surface enhanced NMR spectra of aluminum containing catalytic material, such as γ-alumina,[11,12] as well as mesoporous alumina and aluminum containing metal organic frameworks (MOFs).[13,14] The majority of this work utilizes cross polarization (CP) from ^{1}H to ^{27}Al in conjunction with MAS. This "indirect" method of hyperpolarizing ^{27}Al via the frozen solvent with designer bi-radicals, e.g. TOTAPOL and bTbk, has been shown to yield ^{27}Al signal enhancement factors of 15-20. However, if the objective is to account for surface ^{27}Al species with specific affinity for a paramagnetic labeled reactant, the detection of solvent ^{1}H accessible ^{27}Al species, as captured with CP-DNP, may be of limited interest. This study tests an alternative approach of direct DNP polarization of ^{27}Al via dipolar coupled electron spin probes that are mono-nitroxide-based radical spin probes. By relying on the electron spin of these probes dipolar coupled to the ^{27}Al nuclei, the direct DNP signal enhancement will be weighted towards the aluminum sites in spatial proximity of the mono-

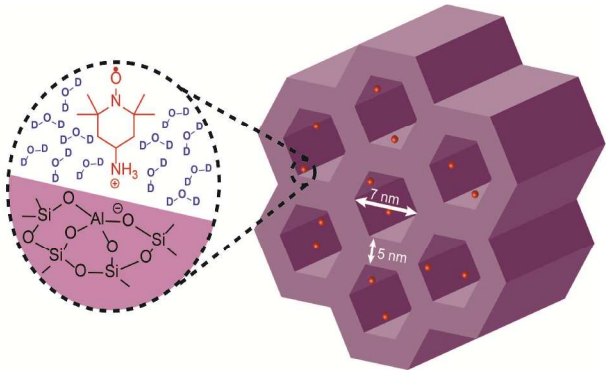

Figure 1. Schematic representation of Al-SBA-15 (Si/Al~20) with 4-amino TEMPO imbibed into the pores. The positive charge on the amine group is electrostatically attracted to the negatively charged Al(IV) acid site on the surface of the material.

radical spin probes. The information gained from direct DNP is expected to be complementary to ^{1}H-^{27}Al CP DNP. CP DNP will reflect on enhancement contrast of the solvent ^{1}H as induced by the different radical species. Thus, even with spatially distinctly located spin probes, efficient ^{1}H nuclear spin diffusion likely will dilute any difference in radical localization, in contrast to direct DNP of isolated nuclei.

Differences in surface enhanced NMR of ^{29}Si species via direct vs indirect (CP) DNP have been observed by Lafon, *et. al.* in synthetic clay nanoparticle and porous silica samples using the bi-radical probe TOTAPOL.[15,16]

Crucially, one can exploit differences in mono-radical probes employed for DNP in their selective partitioning or adsorption to the surface sites of interest directed by the side group's size, charge, shape or chemical property. By exploiting instrumental and methodological advances, as described in previous studies[17–19] of our home-built DNP NMR probe, this study reports on observation of direct ^{27}Al DNP signal amplification of dilute Al sites, namely of Al-SBA-15. This material with a Si/Al=20 was chosen to demonstrate the feasibility of direct DNP to target ^{27}Al nuclei of interest using mono nitroxide radical probes. The sample is an excellent model system given the presence of two distinct aluminum sites, namely a tetrahedral coordinated (IV)Al and octahedral coordinated (VI)Al that can be resolved by ^{27}Al MAS NMR (no DNP) as shown in S.I Figure 2.,

The target of this study is the direct DNP enhancement of surface exposed acid sites, associated with tetrahedral coordinated aluminum, Al(IV) in Al-SBA-15, that carry a negative charge (Figure 1). Here, we present a systematic study of direct ^{27}Al DNP enhancement of Al-SBA-15 by employing three different mono-radical probes of varying charge states. Under the sample impregnation condition used here with solution at neutral pH, 4-amino TEMPO (4-AT) is expected to be positively charged, and therefore electrostatically attracted to the Al(IV) site. The negatively charged 4-carboxy TEMPO (4-CT) should be electrostatically repelled from the negatively charged Al(IV) site and silica surface, while the neutral and hydrophilic 4-hydroxy TEMPO (4-HT) would likely be inside the pores but not adsorbed to the Al(IV) site. This is a simplistic representation of the interactions between the spin probes and the surface of the Al-SBA-15 material as it neglects any interaction between the spin probes and the Si-OH surface groups that may have an effect on the local surface concentration of the spin probes. Testing the validity of the simple model of whether selective partitioning of differentially charged nitroxide radical probes to ^{27}Al surface sites can be achieved, and if so, elucidating the consequences for direct ^{27}Al DNP is the goal of this study. The hypothesis is that direct ^{27}Al DNP will be largely determined by the interaction of the spin probes with the surface aluminum sites and the local concentration around the aluminum sites. Besides

static ^{27}Al DNP, 3-pulse ESEEM[20] and X-band cw EPR analysis were performed on the various spin probes imbibed in Al-SBA-15 to determine the extent of adsorption, interaction strength and local concentration of the nitroxide probes to ^{27}Al surface sites.

Experimental Methods

Sample Preparation for DNP/NMR and EPR measurements. The synthesis of the Al-SBA-15 mesoporous material followed the direct synthesis reported by Ying *et al*.[21] The synthesis and characterization of the Al-SBA-15 are detailed in the supporting information, including a 1-D ^{27}Al MAS NMR spectrum acquired at 7 T to demonstrate the presence of both the (IV)Al and the (VI)Al sites in the material (S.I. Figure 2). Samples for DNP/NMR and EPR measurements were prepared with various nitroxide radicals; 4-amino TEMPO (4-AT), 4-carboxy TEMPO (4-CT), and 4-hydroxy TEMPO (4-HT), are imbibed via the incipient wetness method, as described by Emsley and co-workers.[22] The imbibed radical solution was prepared by making a 10 mM solution of the nitroxide radical in either H_2O of D_2O as the solvent. For the incipient wetness method, 60 µL of radical solution was pipetted onto 20 mg of Al-SBA-15. The radical solution and Al-SBA-15 material were stirred until a wet powder was formed.

Static DNP/NMR Instrument and Measurements. For DNP/NMR measurements the wet Al-SBA-15 powder was transferred to a Teflon sample cup and placed in a home-built NMR probe with a 1-loop saddle coil to resonate at 78.2 MHz. The probe was placed inside a custom Janis STVP-NMR cryostat, operating in continuous flow mode. The necessary components for 200 GHz DNP have been described in a previous publication.[17] Most importantly a tunable 200 GHz solid state microwave source (VDI) with a frequency range of 193-201 GHz and a power output of 70 mW was used in conjunction with low loss quasi-optic bridge (~1dB) to couple the microwave to the corrugated waveguide of the NMR/DNP probe. The NMR/DNP signal is measured in the bore of a Bruker Biospin 7 T superconducting magnet with a 300 Avance solution state spectrometer. All DNP/NMR measurements were performed at a temperature of 4 K. The temperature was monitored to be stable within ±0.1 K for all ^{27}Al DNP NMR measurements. DNP measurements were performed with the use of a saturation recovery solid echo pulse sequence

(S.I. Figure 3) while continuously irradiating with microwaves to obtain the DNP enhanced ^{27}Al signal, or without microwave to obtain the unenhanced ^{27}Al NMR signal. The ^{27}Al signal enhancement factor (ε) was calculated by the ratio of $\varepsilon = S_{DNP}/S_{NMR}$, where S_{DNP} is the ^{27}Al signal area while continuously irradiating with microwaves and S_{NMR} is the signal area in the absence of microwaves. All DNP/NMR measurements were taken with a recovery delay time of 60 s. A 60 s recovery time is dramatically shorter than the full build up time of ^{27}Al NMR signal, which can be on the order of hundreds of seconds at 4 K, but detectable signal enhancement is observed already at 60 s recovery time. The DNP enhancement profiles were recorded by measuring the ^{27}Al enhancement as the microwave frequency was stepped from 197 to 199 GHz.

ESEEM Instrument and Measurements. The Al-SBA-15 samples were prepared for ESEEM measurements in the same manner as described above; a 1 mM radical concentration was used in the imbibed solution with H_2O as a solvent. A lower spin probe concentration was used for the ESEEM measurements to insure that the decay of the electron echo, which decays with T_1 of the electron, was long enough to observe modulations of the echo decay. In contrast to DNP measurements, a protonated instead of deuterated solvent must be used for the ESEEM measurements as the modulation frequency of the electron echo decay from deuterium has a similar frequency (2.3 MHz) as Si (2.8 MHz) and Al (3.6 MHz), so that D_2O would obscure the modulations due to the Si and Al in the Al-SBA-15 matrix. All ESEEM experiments were measured at 50 K at 0.35 T with a MS3 resonator on an Elexsys E580 pulse EPR spectrometer at 9.2 GHz. A 3-pulse ESEEM experiment was used (S.I. Figure 6) with a (τ= 140 ns) time selected to optimize the ^{27}Al modulation, the $\pi/2$ pulse was optimized at 16 ns. The peak echo intensity was measured as the variable delay was increased starting at 40 ns and increased in steps of 32 ns. Plotting the echo intensity as a function of variable delay yields a decay that is modulated by the Larmor frequencies of the nuclei coupled to the electron. A representative ESEEM trace is shown in S.I. Figure 6. All ESEEM traces were processed in the same manner; the background decay as fit to a 9th order polynomial a subtracted out and normalized by the polynomial decay. A sin bell window was applied and the real FFT was taken to yield the ESEEM spectrum.

cw EPR Instrument and Measurements. All 9.5 GHz cw EPR measurements were performed at room temperature. The Al-SBA-15 sample with imbibed radical was prepared in the same method as described above. The sample was then placed in a quartz tube and in the center of a dielectric microwave resonator (Bruker ER-4123D). The cw spectra were measured with a Bruker EMX spectrometer at 0.35 T and 9.5 GHz EPR.

Results and Discussion

For direct DNP measurements, pure D_2O was chosen as a solvent to suppress polarization transfer and leakage via ^{1}H nuclear spin diffusion in H_2O. The use of D_2O as a solvent was found to nearly double the ^{27}Al enhancement factors compared to in H_2O solvent (see S.I. Figure 4). This is consistent with observations in the literature, where deuteration of solvent and ^{1}H on protein samples were found to increase the direct ^{13}C DNP enhancement when using a mono- and bi-tempo radical derivative.[23,24] Figure 2 compares the direct ^{27}Al DNP spectra obtained from a single scan with 4-AT, 4-CT, and 4-HT, which

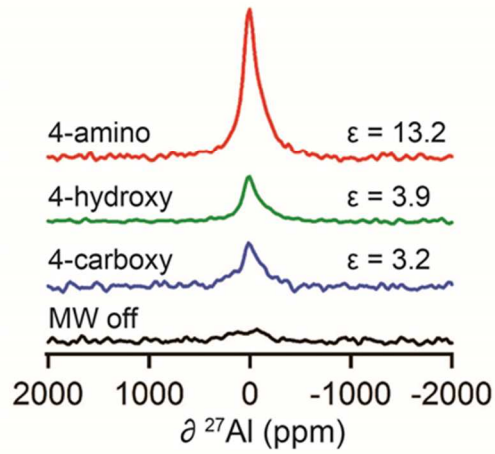

Figure 2. ^{27}Al Direct DNP spectra of Al-SBA-15 imbibed with various 10 mM mono nitroxides spin probe solutions using D_2O as the solvent. The DNP enhanced spectra were measured with irradiation at a microwave frequency where the maximum positive enhancement occurs for each spin probe (197.7 GHz for 4-AT, 197.75 GHz for 4-HT and 4-CT).

were found to be ε = 13.2, ε = 3.2, and ε = 3.9 respectively. 4-AT was chosen as a spin probe that would likely target the active aluminum sites in Al-SBA-15 mediated by electrostatic attraction to the negatively charged Al(IV). Thus, the question to be addressed is whether the highest enhancements seen with 4-AT is due to the proximity, and by extension stronger dipolar coupling, between surface ^{27}Al species and

adsorbed 4-AT. For this, experimental evidence for surface adsorption and ^{27}Al-electron proximity is needed and will be addressed in the following sections.

When employing nitroxide radicals as DNP polarizing agents, it has been shown that the width and detailed shaped of the microwave frequency-dependent DNP enhancement profile contains key information about the DNP mechanism.[25–27] When combined with quantum mechanically derived spin dynamics calculation, the % contribution of cross effect (CE) or solid effect (SE) DNP mechanism can be extracted, as well as the effect of EPR spectral diffusion simulated.[28] However, even when measuring simply the frequency difference between the DNP maxima, Δ_{DNP}, one can extract whether a dominant CE, SE or mixed effect is at play. If the Δ_{DNP} equals twice the nuclear Larmor frequency, ω_n, likely the SE is dominant, although this is only unambiguous if ω_n exceeds the EPR spectral width.[29] If Δ_{DNP} does not equal $2\omega_n$ and the DNP maxima lie within the EPR line, then the CE is likely the dominant mechanism. Here we do not discuss the thermal mixing (TM) mechanism based on the results of Hovav et. al.[30] where it was observed that in mono-nitroxide frozen solutions under static conditions at similar concentrations and liquid helium temperatures, the electron spin polarization distribution is not described with a cooled Zeeman spin temperature.

Figure 3 shows representative frequency profiles for the direct DNP enhancement of ^{27}Al when employing 4-AT and 4-CT. The shape of the DNP frequency profile, with positive signal enhancement at

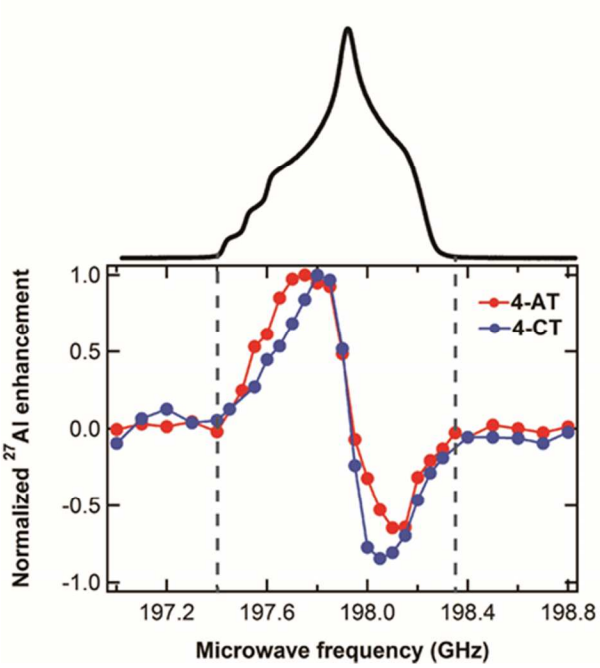

F igure 3. Shown are ^{27}Al DNP frequency profile of 4-AT and 4-CT imbibed in Al-SBA-15. 4-HT yielded a comparable frequency profile and peak to peak width as 4-CT. A representative nitroxide EPR spectrum is shown above, measured at 8.56 T as described in the supporting information. The dashed lines represent the edge of the EPR line, demonstrating that the DNP frequency profiles of 4-AT and 4-CT fall within the nitroxides EPR line.

microwave frequencies below the central EPR transition, zero enhancement when the microwave frequency is at the central EPR transition, and negative signal enhancement at microwave frequencies larger than the EPR central transition, firmly establishes that the observed enhancements are caused by a DNP process and not by a decrease in relaxation time due to heating effects when the sample is irradiated with microwaves. The Δ_{DNP} of 4-AT is 350 MHz ± 50, the Δ_{DNP} of 4-CT and 4-HT is ~250 ± 50 MHz. The bumps visible in the baseline of 4-CT enhanced ^{27}Al spectrum at 197.2 GHz and 198.7 GHz are likely artifacts due to the low signal to noise ratio. Thus, all Δ_{DNP} values are much larger than 2 times ω_n of the ^{27}Al NMR Larmor frequency (ω_n = 78.2 MHz at 7 T), while also falling within the nitroxide EPR spectral width, as explicitly measured and displayed above the DNP frequency profiles. The EPR absorption line was measured directly using a rapid passage method detailed in the supporting information. From this we conclude the DNP with all three mono-nitroxide probes dominantly proceeds via the CE mechanism. When comparing the DNP frequency profiles, it is clear that Δ_{DNP} is largest for 4-AT. Within the CE DNP mechanism, it has been shown recently that increasing the radical concentration broadens the DNP profile as measured by an increase in Δ_{DNP} due to stronger electron-electron dipolar coupling between proximal electron spins.[27] The increased Δ_{DNP} of 4-AT can thus be attributed to an increased local spin concentration at the surface of the Al-SBA-15 relative to that of 4-CT or 4-HT, despite the same overall spin concentration of the 10 mM solution imbibed in each sample; suggesting that 4-AT does show an increased attraction to the surface of the Al-SBA-15 material as purposed.

In order to independently and directly test whether the 4-AT species is indeed closer specifically to surface ^{27}Al species than the other spin probes, 3-pulse ESEEM was used to directly measure the strength of the coupling of each spin probe to the ^{27}Al and ^{29}Si in the material (SI Figure 4 shows a three pulse ESEEM sequence). This pulsed EPR technique monitors the electron spin echo decay, whereby for 3-pulse ESEEM the echo decay is influenced by the T_1 of the electrons, as well as the spectral and spin diffusion of the electron spins. If (weak) anisotropic coupling between the electron spin and nearby nuclei is present, this echo decay is further modulated by the nuclear Larmor frequencies of the proximal nuclei. A representative ESEEM echo decay for nitroxide spin probes imbibed in Al-SBA-15 is shown in SI Figure 4. In the case of weak hyperfine coupling, the modulation depth is dependent on the electron nuclear distance, the number of nuclei around the spin probe, and the nuclear spin type.[31,32] When the modulation

depth is large, it can be directly extracted from the ESEEM time trace.[33,34] However in our case, when many nuclei are weakly interacting with the spin probes, the modulation depths of the ^{27}Al and ^{29}Si are shallow and cannot be directly extracted from the ESEEM time trace. Rather, we can compare the intensity of the ^{27}Al (I_{Al}) and ^{29}Si (I_{Si}) in the Fast Fourier Transform (FFT) of the ESEEM trace for each spin probe as a comparative measure of the modulation depth that will reflect on the strength of the electron nuclear interaction.[35] Even though it is known that ^{27}Al can have a large quadrupolar interaction that affects the intensity of the ESEEM spectrum, it has been shown when comparing different spin probes in the same aluminum material system for weakly coupled aluminum nuclear spins, that the quadrupolar interaction does not change when varying the spin probe type.[31]

The ESEEM time traces were processed in a similar manner as described by Carmieli et. al.,[33] which is detailed in the S.I. Figure 4a shows the ESEEM spectrum for the different spin probes when imbedded in Al-SBA-15. The interactions of the spin probes with ^{29}Si and ^{27}Al in the Al-SBA-15 framework are shown by the peaks at 2.88 MHz and 3.66 MHz respectively. The peak a 14.04 MHz results from the spin probes interaction with ^{1}H from largely the solvent. Figure 4b shows a plot of the I_{Al} and I_{Si} for each spin probe imbibed in Al-SBA-15. Information about the spin probes location on the overall surface of Al-SBA-15 can be inferred from the I_{Si}. We find I_{Si} is the largest for 4-AT out of all the spin probes, smaller for 4-HT, and yet smaller for 4-CT. This indicates that 4-AT yields a larger ^{29}Si modulation depth and shows a stronger interaction with the surface silica than both 4-HT and 4-CT, where the strength of the interaction between the spin probes and the ^{29}Si species can be ranked 4-AT>4-HT>4-CT. Looking to figure out whether 4-AT not only is enriched at the silica surface, but also targets surface ^{27}Al sites, we turn to I_{Al}. Indeed, the I_{Al} is the largest for 4-AT out of all the spin probes while the I_{Al} of 4-HT and 4-CT is very similar with 4-HT. Thus from the ESEEM spectrum we can rank the interaction of the spin probes with surface ^{27}Al species as 4-AT>4-HT≈4-CT. This suggests that 4-AT does have the largest population localized on the surface of the material yielding a larger I_{Al} and I_{Si} than either of the other two radicals. Conversely, 4-CT has the smallest localize population on the surface of the material, suggested by the smallest I_{Al} and I_{Si}. This matches the ^{27}Al DNP enhancement trend, suggesting that the larger enhancement from 4-AT comes from a higher local surface concentration and accordingly a closer average proximity to ^{27}Al. Delineating between these two factors is nontrivial, however, clearly 4-AT show

a significantly stronger interaction with the surface aluminum sites of Al-SBA-15 than the other two radicals. The latter is key because this implies that characterization of the surface aluminum sites

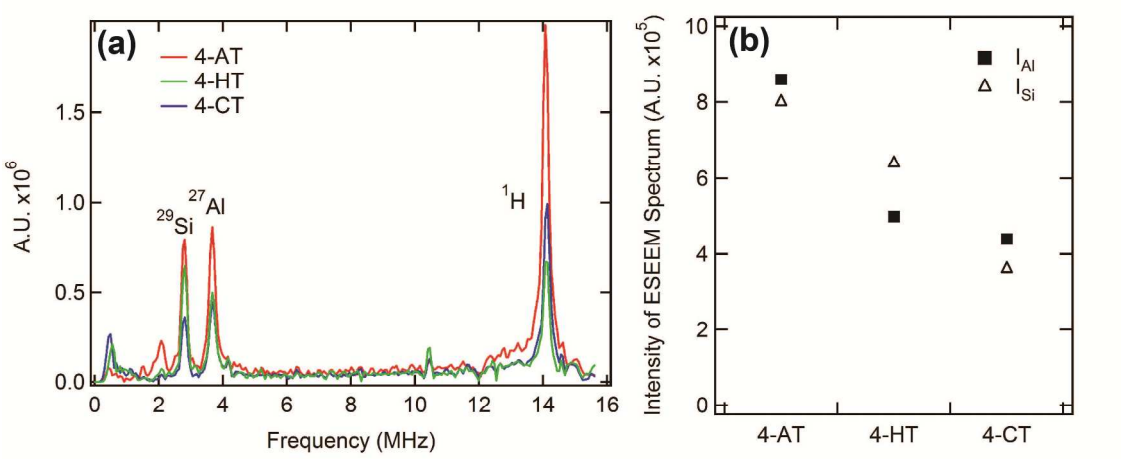

Figure 4. (a) The ESEEM spectrum for the various mono nitroxides radicals. The peak at close to zero frequency is an artefact that comes from the baseline correction process of the time domain ESEEM trace. **(b)** I_{Al} and I_{Si} for each nitroxide radical, due to similar linewidth between each radical, the peak height was taken as the measurement of intensity rather than the integral of the peak.

accessible to a radical-labeled reactant molecule may be feasible in future work.

To directly demonstrate the physical adsorption of 4-AT to the surface of Al-SBA-15, cw EPR lineshape analysis was performed at 9.5 GHz and room temperature for all three radicals. Figure 4 shows a representative cw EPR spectrum of each spin probe imbibed in Al-SBA-15. In the EPR spectrum of 4-AT and 4-CT (Figure 5a, 5b) two populations are present: an immobile and mobile spectral component, represented by the intensities I_{imm} (red arrow) and I_{mob} (green arrow). The broad immobile component of the cw EPR spectra is attributed to spin probe adsorbed to the surface of Al-SBA-15, while the mobile component is attributed to spin probe tumbling freely in the pores of the material. When comparing the ratio of the I_{imm}/I_{mob} it is clear that 4-AT has the largest proportion of its population adsorbed to the surface of the Al-SBA-15, with an I_{imm}/I_{mob}=0.2, compared to 4-CT (I_{imm}/I_{mob}=0.08) and 4-HT (Figure 5c) which showed no immobile population (see detailed discussion on I_{imm}/I_{mob} as a function of loaded spin probe concentration in SI).

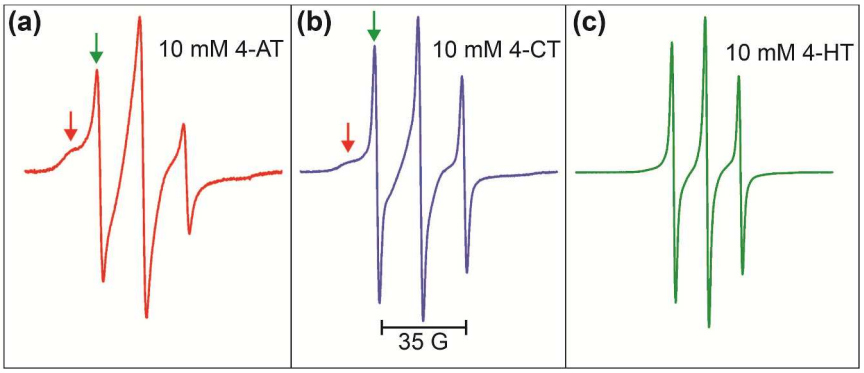

Figure 5. X-band CW EPR spectra of 10 mM **(a)** 4-AT, **(b)** 4-CT, and **(c)** 4-HT imbibed in Al-SBA-15. Two spin probe populations can be seen in 4-AT and 4-CT; immobile (red arrow) and mobile (green arrow) component.

Conclusion

By concurrently analyzing the DNP frequency profile, and the cw EPR lineshape of imbibed spin probes, we find that 4-AT has the largest surface-adsorbed population, indicating a higher local surface concentration when compared to 4-CT and 4-HT, which likely plays a role in determining its favorable DNP enhancement factor. More importantly, the ESEEM spectrum of 4-AT when compared with the other spin probes showed the strongest interaction specifically with the surface ^{27}Al species compared to 4-CT and 4-HT. This is the first study demonstrating the viability of targeted DNP characterization by varying the functional side groups of mono-radical spin probes. As such, it represents an important stepping-stone towards the characterization of materials surfaces “as seen by probes”. In the future, reactants and other potent chemical moieties can be spin labeled for targeted surface characterization of active sites or surfaces of interest. In order to definitively address the ultimate question of whether 4-AT selectively enhances the Al(IV) acid site over other present aluminum species in Al-SBA-15, MAS DNP must be implemented to obtain chemical shift resolution. MAS-DNP at temperatures less than 20-30 K might be desirable in order to work with dilute ^{27}Al concentrations as typical for samples relevant to catalysis. Such studies of direct surface aluminum site-specific enhancement by MAS-DNP are underway and will be the topic of future publications.

Acknowledgements

This study was primarily funded by the National Science Foundation (CHE #1112572) awarded to Songi Han. We would like to acknowledge Prof. Bradley Chmelka for supplying Al-SBA-15 material and Prof. Daniella Goldfarb for helpful discussions on ESEEM experiments. We would also like to thank Dr. Kuo-Ying Huang and Dr. Jinsuk Song for help with the solid state NMR and cw EPR experiments. The MRL Shared Experimental Facilities are supported by the MRSEC Program of the NSF under Award No. DMR 1121053; a member of the NSF-funded Materials Research Facilities Network (www.mrfn.org).

(1) Perego, C.; Millini, R. *Chem. Soc. Rev.* **2013**, *42*, 3956–3976.

(2) Engelhardt, G.; Michel, D. *High-Resolution Solid-State NMR of Silicates and Zeolites*; John Wiley & Sons: Norwich, 1987.

(3) Chiu, J. J.; Pine, D. J.; Bishop, S. T.; Chmelka, B. F. *J. Catal.* **2004**, *221*, 400–412.

(4) Hu, W.; Luo, Q.; Su, Y.; Chen, L.; Yue, Y.; Ye, C.; Deng, F. *Microporous Mesoporous Mater.* **2006**, *92*, 22–30.

(5) Serrano, D. P.; Aguado, J.; Escola, J. M. *ACS Catal.* **2012**, *2*, 1924–1941.

(6) Werner, M.; Rothermel, N.; Breitzke, H.; Gutmann, T.; Buntkowsky, G. *Isr. J. Chem.* **2014**, *54*, 60–73.

(7) Jiang, Y.; Huang, J.; Dai, W.; Hunger, M. *Solid State Nucl. Magn. Reson.* **2011**, *39*, 116–141.

(8) Wischert, R.; Florian, P.; Copéret, C.; Massiot, D.; Sautet, P. *J. Phys. Chem. C* **2014**, *118*, 15292–15299.

(9) Hall, D. A.; Maus, D. C.; Gerfen, G. J.; Inati, S. J.; Becerra, L. R.; Dahlquist, F. W.; Griffin, R. G. *Science* **1997**, *276*, 930–932.

(10) Rossini, A. J.; Zagdoun, A.; Lelli, M.; Lesage, A.; Copéret, C.; Emsley, L. *Acc. Chem. Res.* **2013**, *46*, 1942–1951.

(11) Vitzthum, V.; Mieville, P.; Carnevale, D.; Caporini, M. A.; Gajan, D.; Coperet, C.; Lelli, M.; Zagdoun, A.; Rossini, A. J.; Lesage, A.; Emsley, L.; Bodenhausen, G. *Chem. Commun.* **2012**, *48*, 1988–1990.

(12) Lee, D.; Duong, N. T.; Lafon, O.; De Paëpe, G. *J. Phys. Chem. C* **2014**, *118*, 25065–25076.

(13) Lee, D.; Takahashi, H.; Thankamony, A. S. L.; Dacquin, J.-P.; Bardet, M.; Lafon, O.; Paëpe, G. De. *J. Am. Chem. Soc.* **2012**, *134*, 18491–18494.

(14) Pourpoint, F.; Thankamony, A. S. L.; Volkringer, C.; Loiseau, T.; Trebosc, J.; Aussenac, F.; Carnevale, D.; Bodenhausen, G.; Vezin, H.; Lafon, O.; Amoureux, J.-P. *Chem. Commun.* **2014**, *50*, 933–935.

(15) Lafon, O.; Thankamony, A. S. L.; Rosay, M.; Aussenac, F.; Lu, X.; Trebosc, J.; Bout-Roumazeilles, V.; Vezin, H.; Amoureux, J.-P. *Chem. Commun.* **2013**, *49*, 2864–2866.

(16) Lafon, O.; Rosay, M.; Aussenac, F.; Lu, X.; Trébosc, J.; Cristini, O.; Kinowski, C.; Touati, N.; Vezin, H.; Amoureux, J.-P. *Angew. Chemie Int. Ed.* **2011**, *50*, 8367–8370.

(17) Armstrong, B. D.; Edwards, D. T.; Wylde, R. J.; Walker, S. A.; Han, S. *Phys. Chem. Chem. Phys.* **2010**, *12*, 5920–5926.

(18) Siaw, T. A.; Walker, S. A.; Armstrong, B. D.; Han, S.-I. *J. Magn. Reson.* **2012**, *221*, 5–10.

(19) Walker, S. A.; Edwards, D. T.; Siaw, T. A.; Armstrong, B. D.; Han, S. *Phys. Chem. Chem. Phys.* **2013**, *15*, 15106–15120.

(20) Schweiger, A.; Jeschke, G. *Principles of Pulsed Electron Paramagnetic Resonance*; Oxford University Press: New York, 2001.

(21) Li, Y.; Zhang, W.; Zhang, L.; Yang, Q.; Wei, Z.; Feng, Z.; Li, C. *J. Phys. Chem. B* **2004**, *108*, 9739–9744.

(22) Rossini, A. J.; Zagdoun, A.; Lelli, M.; Gajan, D.; Rascon, F.; Rosay, M.; Maas, W. E.; Coperet, C.; Lesage, A.; Emsley, L. *Chem. Sci.* **2012**, *3*, 108–115.

(23) Lumata, L.; Merritt, M. E.; Kovacs, Z. *Phys. Chem. Chem. Phys.* **2013**, *15*, 7032–7035.

(24) Akbey, Ü.; Franks, W. T.; Linden, A.; Lange, S.; Griffin, R. G.; van Rossum, B.-J.; Oschkinat, H. *Angew. Chemie Int. Ed.* **2010**, *49*, 7803–7806.

(25) Hovav, Y.; Feintuch, A.; Vega, S. *Phys. Chem. Chem. Phys.* **2013**, *15*, 188–203.

(26) Mak-Jurkauskas, M. L.; Griffin, R. G. In *eMagRes*; John Wiley & Sons, Ltd, 2007.

(27) Siaw, T. A.; Fehr, M.; Lund, A.; Latimer, A.; Walker, S. A.; Edwards, D. T.; Han, S.-I. *Phys. Chem. Chem. Phys.* **2014**, *16*, 18694–18706.

(28) Shimon, D.; Hovav, Y.; Feintuch, A.; Goldfarb, D.; Vega, S. *Phys. Chem. Chem. Phys.* **2012**, *14*, 5729–5743.

(29) Wind, R. a; Zumbulyadis, N.; Young, R. H.; Hung, Y.; Li, L.; Nuttall, R. H.; Maciel, G. *Solid State Nucl. Magn. Reson.* **1992**, *1*, 55–65.

(30) Hovav, Y.; Kaminker, I.; Shimon, D.; Feintuch, A.; Goldfarb, D.; Vega, S. *Phys. Chem. Chem. Phys.* **2015**, *17*, 226–244.

(31) Caragheorgheopol, A.; Rogozea, A.; Ganea, R.; Florent, M.; Goldfarb, D. *J. Phys. Chem. C* **2009**, *114*, 28–35.

(32) Kevan, L. In *Time Domain Electron Spin Resonance*; John Wiley & Sons, 1979; pp. 280–311.

(33) Carmieli, R.; Papo, N.; Zimmermann, H.; Potapov, A.; Shai, Y.; Goldfarb, D. *Biophys. J.* **2006**, *90*, 492–505.

(34) Ionita, G.; Florent, M.; Goldfarb, D.; Chechik, V. *J. Phys. Chem. B* **2009**, *113*, 5781–5787.

(35) Baute, D.; Goldfarb, D. *J. Phys. Chem. C* **2007**, *111*, 10931–10940.